
Proceedings Paper:
Hardy, M.C., Argyrakis, C., Kitaguchi, H.S. et al. (17 more authors) (2020) Developing alloy compositions for future high temperature disk rotors. In: Tin, S., Hardy, M., Clews, J., Cormier, J., Feng, Q., Marcin, J., O'Brien, C. and Suzuki, A., (eds.) Superalloys 2020 : Proceedings of the 14th International Symposium on Superalloys. Superalloys 2020 : 14th International Symposium on Superalloys, 12-16 Sep 2021, Seven Springs, PA, USA. The Minerals, Metals & Materials Series . Springer International Publishing , pp. 19-30. ISBN 9783030518332

https://doi.org/10.1007/978-3-030-51834-9_2

Developing Alloy Compositions for Future High Temperature Disk Rotors

M. C. Hardy, C. Argyrakis, **H.** S. Kitaguchi, A. S. Wilson, R. C. Buckingham, K. Severs, S. Yu, C. Jackson, **E. J.** Pickering, S. C. **H.** Llewelyn, C. Papadaki, K. A. Christofidou, P. M. Mignanelli, A. Evans, D. **J. Child, H. Y. Li,** N. G. Jones, C. M. F. Rae, P. Bowen, and **H.** J. Stone

Abstract

Two new alloy compositions for possible disk rotor applications have been examined. Both were intended to have higher γ' content than the existing alloy, RR lO00, and be produced using powder metallurgy and isothermal forging to enable forgings to show a consistent coarse grain microstructure. Small pancake forgings of the new alloys and RRlO00 were made and from these, blanks were cut, solution heat treated, cooled at measured rates and aged. Results of screening tests to understand the tensile, creep and dwell crack growth behavior, oxidation resistance and phase stability of these new alloys and coarse grain RRlO00 are reported. The development alloys were similar in composition but exhibited different tensile and creep properties, phase stability and resistance to oxidation damage. Despite attempts to minimize variation in microstructure from heat treatment, differ- ences in γ' size distribution were found to influence tensile and creep behavior. One of the new alloys (Alloy 2) showed improved yield and tensile strength compared to RRlO00. Alloy 2 displayed similar initial creep strain behavior to RRl000 but superior resistance to subsequent creep damage , producing longer creep rupture lives. All of the alloys showed crack retardation at low stress intensity factor ranges (LlK) from 3600 s dwell cycles at 700 °C in air. This occurred whilst crack growth was intergranular. Alloy 1 was found to precipitate C14 Laves phase from long term exposure at 800 °C. Like RRlO00, cT phase was not detected in the new alloys after 750 h at 800 °C.

M. C. Hardy (18J) · C. Argyrakis · R. C. Buckingham · P. M. Mignanelli · D. J. Child
Rolls-Royce Pie, Derby, UK
e-mail: mark . har dy@rolls- royce.com

A. S. Wilson · K. A. Christofidou · N. G. Jones · C. M. F. Rae · H. J. Stone
Department of Materials Science and Metallurgy, University of Cambridge, Cambridge, UK

H. S. Kitaguchi · S. Yu · C. Jackson · S. C.H. Llewelyn · H. Y. Li · P. Bowen
School of Materials and Metallurgy, University of Birmingham, Binningham, UK

K. Severs
Allegheny Technologies Incorporated (ATl) Forged Products Cudahy, Cudahy, WT, USA

A. Evans
Bundesanstalt Fiir Materialforschung Und -Priifung (BAM), Berlin, Germany

E. J. Pickering
Department of Materials, University of Manchester, Manches ter, UK

C. Papadaki
Department of Engineering Science, University of Oxford, Oxford , UK

Keywords

Powder metallurgy • Phase stability • CALPHAD • Material properties

Introduction

High bypass ratio turbofan aircraft engines and operating cycles are continuously evolving to provide improved effi- ciencies for reduced fuel consumption and emissions [1, 2]. However, whilst propulsive and aerodynamic optimizations of aircraft engines are possible, the increased demands upon superalloys, which are used in the hot section parts, limit the thermal efficiency improvements that can be achieved. The requirements for reduced engine core sizes and increased temperatures and stresses pose a complex set of seemingly conflicting property requirements for the materials consid- ered for safety-critical disk rotor applications. Specifically, materials with higher strength levels are needed to reduce the size and weight of components. Whilst this necessitates the

development of compositions with increased amounts of the gamma prime (γ′) phase, further optimization is possible by using a fine grain size. Yet such grain structures produce less appealing time dependent crack growth behavior [4], which may limit the design life of the component or the interval between inspections. This is more relevant in today′s engi- nes as high climb rates are increasingly required by com- mercial airlines to move aircraft more quickly to altitude to reduce fuel bum [5]. Therefore acceptable strength is required from coarse grain mic rostruct ures, which demands effective precipitation strengthening from alloy design and control of grain size in near net shaped forgings.

Inevitably, this is only possible using powder metallurgy to minimize elemental segregation to length scales of a micron (μm) or less for these complex, multi-component alloys with high levels of reactive elements (Al, Ti, Ta etc.) [6- 8]. Subsequent hot deformation of consolidated powder compacts produces billet material with extremely fine grains, which enables superplastic flow of the work piece during isothermal forging at high temperatures and low strain rates, to make the desired near net disc shapes [6- 8]. A uniform average grain size of 20-40 μm can then be created by super-solvus solution heat treatment. This microstructure produces an ideal balance in material properties between tensile strength and resistance to time dependent crack growth. Otherwise , optimization of strength in the hub of the disc and resistance to time dependent crack growth and creep in the rim and diaphragm can be achieved by producing dual microstructure forgings, albeit with greater design and manufacturing complexity as well as increased cost [4].

To achieve the desired material properties, careful con-sideration is required of the volume fraction, number den- sity, size and morphology of γ′ precipitates, as well as the heat treatments and rates of cooling that produce these. Alloy design and development is further complicated by minor grain boundary phases, surface degradation from oxidation and type II hot corrosion, coarsening and disso- lution of γ′ particles and possible precipitation of detrimental topologically close packed (TCP) phases as a result of long duration exposures at temperatures above 700 °C.

This paper discusses the design of 2 development alloys and evaluates their microstructure and material properties, comparing them against an existing Rolls-Royce alloy , RRlO00 [9].

Alloy Design

The first priority in designing the new alloys was to achieve the required yield strength in a coarse grain microstructure. Of the strengthening mechanisms that give rise to the per-formance of nickel base superalloys, precipitation hardening is the most significant. Strengthening occurs as a result of creating fault energies from anti-phase boundaries and stacking faults when paired dislocations penetrate γ′ parti-cles. It is understood then that a new alloy should contain a larger number density of (preferably smaller) γ′ particles, compared to existing alloys to provide a higher level of precipitation hardening . This understanding is formalized in models that are available in the literature [10- 14]. These correlate the critical resolved shear stress or flow stress of the alloy with the volume fraction and size of γ′ particles, and the anti-phase boundary (APB) energy. In practice, the new alloys in this study (Table 1) were designed by specifying a volume fraction of γ′ of about 50- 53%. It was considered that this range should produce sufficient levels of improve-ment over the existing alloy , RRlO00, which has 45% γ′ , but without incurring significant detriments to time dependent crack growth behavior or difficulties in raw material and component manufacture.

As γ′ is described by Ni_3X, where *X* is predominantly Al with progressively smaller proportions of Ti, Ta and Nb, the specified volume fraction of γ′ was defined according to:

$$13.15 \text{ atomic\%} > \text{Al} + \text{Ti} + \text{Ta} + \text{Nb} > 12.65 \text{ atomic\%} \quad (1)$$

and elemental ranges of 6.55 to 7.15 at. % for Al, 3.3 to 3.7 at. % for Ti, 1.2 to 1.7 at. % for Ta and 0.8 to 1.0 at. % for Nb. These ranges were determined [15- 17] by considering the effect of these elements on (i) strengthening potential (or APB energy), (ii) the γ′ dissolution or solvus temperature (Tsolvus), (iii) the propensity for eta (T]) formation, (iv) the stability of primary MC carbides, (v) oxidation resistance (notably Ti), and (vi) dwell crack growth behavior (notably Nb).

The first 4 of these factors (i-iv) were assessed using phase diagram modelling [18- 20] and Thermo-Cale data- bases TCNi6 and 7. These were the current databases when the development alloy s were designed . The work of Crudden et al. [13] was also influential in optimizing strengthening

Table 1 Nominal compositions (in atomic percent) of development alloys [15- 17] and RRlO00 [9]

at.%	Ni	Co	Cr	Mo			Mn	Al	Ti	Ta	Nb	Si	Hf	B	C	Zr
Alloy 1	Bal.	15.0	14.0	1.3			0.6	7.0	3.5	1.6	0.9	0.90	0	0.14	0.15	0.05
Alloy 2	Bal.	15.6	14.0	1.4	1.1	1.0	0	6.8	3.5	1.6	0.9	0.32	0	0.14	0.15	0.06
RRI000	Bal.	17.9	16.5	3.0	0	0	0	6.4	4.3	0.6	0	0	0.1 6	0.08	0.13	0.03

potential. They showed that the composition of the γ' particles, i.e. the concentration of Ti, Ta and Nb atoms that replace Al atoms, has a profound effect on the APB energy and therefore yield stress. Tsol vus was important in the alloy design to ensure that forgings, which will receive a super-solvus solution heat treatment to produce a coarse grain microstructure, do not suffer from incipient melting at grain boundaries and quench cracking. This is particularly problematic in alloys that contain high levels of γ' and B. The risk was minimized by limiting T,o l vus to values of about 1165 °C. Whilst Co and Cr also have significant influence on T,o l vus, this target value principally restricted the Al content. The Ti ranges were then selected to improve oxidation resistance (which was correlated to the Cr/Ti ratio in at. %), to avoid T] formation, to minimize Tso lvu s and to maintain a stable MC carbide in alloys with Ta and Nb. Specifically, Antonov et al. [21] have shown that T] and delta (o) phase can be avoided by ensuring that the Al, Ti, Ta and Nb values in atomic % are such that:

$$\frac{\text{Al}}{\text{T1+ Ta + Nb}} > 0.85 \quad (2)$$

Tantalum and Nb were added to the development compositions at appropriate levels to satisfy Eqs. (1) and (2) with the caveat that Nb be limited to 1 at.% (about 1.6 weight %) as there were concerns that excess Nb would be detrimental to time dependent crack growth. This limit was considered to be safe, albeit conservative as evidence in the literature [22] indicates that the effect of Nb content (up to about l. 7 wt%) on dwell crack growth behavior is less significant than grain size and size of γ' precipitates. The presence of Ta and Nb in γ' was understood to be beneficial as these elements show slower rates of diffusion in Ni compared to Al and Ti, which reduces coarsening during material manufacture and com- ponent operation. It was also considered that sufficient quantities of Ta and Nb should be added to the new alloys to develop stable MC carbides (where M can be Ti, Ta or Nb), which would resist decomposition at lower temperatures to $M_{23}C_6$ carbides. These latter grain boundary carbides were regarded as detrimental as they remove Cr from the y matrix adjacent to grain boundaries [23], reduce oxidation resis- tance and elevated temperature fatigue crack nucleation life [24]. Unlike Ti and Nb (due to large volume changes from forming Nb_2O_5 [25]), Ta may not be detrimental to oxida- tion resistance and has been shown to improve time dependent crack growth resistance [26]. The negative impact of adding Ta is the increase in raw material cost and with Nb, the increase in density .

Yield stress models are more useful if they include terms for grain size (d) and the size of secondary γ' particles, *i.e.* those produced from quenching after solution heat treatment. The model shown below, proposed by Parthasarathy et al. [11] was used in comparing the yield stress of new compositions with those of established alloys.

$$\sigma_y = \left(1 - f_{\gamma}'\right)\left\langle M(CRSS) + \frac{k_{(\gamma+\gamma')}}{\sqrt{d_{(\gamma+\gamma')}}}\right\rangle + f_{\gamma'}\left\{M \times \tau_{\gamma}' + \frac{k_{\gamma}'}{\sqrt{d_{\gamma}'}}\right\} \quad (3)$$

where $f_{\gamma'}$ is the volume fraction of γ' particles, CRSS is the critical resolved shear stress, M is the Taylor factor for polycrysta ls, dis grain size, k is the Hall-Petch coefficient for y and γ' phases and r . is the friction stress that opposes dislocation motion from grain boundary precipitated γ' particles. Further details of the model can be found in [27].

More attention was paid to strength of the y phase for producing resistance to creep deformation. Initially, work was conducted to determine a minimum Co content for achieving the required creep strain behavior and a T,o l vus value below 1165 °C. A minimum Co content was sought to reduce the propensity for CT formation [28], to promote improved resistance to type II hot corrosion damage since the melting temperature of Na_2SO_4-$CoSO_4$ eutectic is 565 °C [29], compared to Na_2SO_4- $NiSO_4$, which melts at 671 °C [30], and to minimize raw material costs. The benefits of Co in lowering the stacking fault energy [28, 31] and in producing more annealing twins are well documented [32]. The latter reduces effective grain size, which is important for fatigue crack nucleation life for coarse grain microstructures at temperatures below 650 °C. A further, less established benefit of Co is its ability to influence the size of secondary γ' particles, particularly those in intergranular locations. For a given cooling rate from super-solvus solution heat treatment, increasing Co content reduces the size of secondary γ' precipitates [33].

The other contribution to y strength was provided by Mo and W. Whilst established alloys have shown that high concentrations of Mo and W are necessary for good creep resistance, their values in the development compositions were limited by concerns regarding phase stability and density. Two approaches were used to provide an indication of phase stability was understood in 2 ways, both of which used the results of phase diagram modelling (Table 2). Firstly, to predict the solvus temperature for detrimental TCP phases, notably CT (which is rich in Cr, Mo and W), to ensure that these were minimized and at least below the value for RRIO00. Secondly, predictions of the atomic fraction of elements in the *y* phase were used in the second approach to calculate the average energy of d orbitals of alloying transition metals (Mdy), after Morinaga et al. [34]. The usefulness of this approach relies on defining a critical average Mdy value, below which a CT free microstructure is likel y. Guedou et al. [35] proposed that alloys can be designed using an average Mdy value of 0.915. In latter work, Reed

Table 2 Results of phase diagram modelling for the alloys in Table I , calculated using the Thermo-Cale software with the TCNi7 database

Alloy	Y' Tsolvu s(°C)	Tsolidu s(°C)	cr Tsolvus(°C)	Ave Md r	(%)
Alloy 1	1102	1214	863	0.917	0.04
Alloy 2	1092	1203	847	0.911	0.13
RRlO00	1121	1232	909	0.905	0.08

γ' Tsolvu s and cr Tsolvus are the solvus temperatures for the γ' and cr phases, respectively, and Tsolidus is the incipient melting temperature. Ave Md, is the average energy of *d* orbitals of alloying transition metals, after Morinaga et al. [36], and 8 is the lattice misfit. These were calculated at 600 °C

et al. [3] calculated that alloys for which the average Mdy number was less than 0.88 would be free of er phase. At the concept stage, a value similar to that for RRlO00 was considered acceptable for the development alloys in this current work.

The aim in designing the alloys was to develop low or no coherency strain to minimize coarsening of γ' precipitates during time at temperatures above 700 °C. One measure of coherency strain is lattice misfit (6), given by Eq. (4).

$$\delta = \frac{2\,(a_{\gamma'} - a_{\gamma})}{a_{\gamma'} + a_{\gamma}} \qquad (4)$$

The values of *c5* in Table 2 were estimated for 600 °C using the respective lattice parameters of y (a) and γ′ (a) ,

which were calculated from molar volume values of the phases from phase diagram modelling and Avogadro's constant.

Resistance to environmental damage was sought by reducing the amount of Ti, thereby increasing the Crffi ratio. It is understood that Ti dopes the chromia scale [36], where it segregates primarily along grain boundaries and forms large rutile nodules above the chromia scale [37]. It was found that for RRlO00, the initial rates for the thickening kinetics of the chromia scale are considerably higher than those for relatively Ti-free chromia in alloys such as Inconel 718 and ATI 7l 8Plus™ [36]. For Alloys l and 2 in Table 1, it was proposed that further improvements in resistance to environmental damage could be achieved by adding Si and Mn. Pedrazzini et al. [38] reported that after 100 h at 800 °C, an oxide scale in a Ni-base alloy with l at. % Mn consisted of an outer layer of $NiCr_2Mn_2O_4$ and a subsequent inhomogeneous mix of chromia, spinel $MnCr_2O_4$ and rutile $(Ti,Cr)O_2$. A 3 fold reduction in oxide thickness was observed compared to RRlO00. Whilst this is encouraging, it is unclear whether the reduction was due to the presence of **Mn** or a consequence of the low **Ti** content (1 at. % Ti) and the high Crffi ratio of 16.

The beneficial effects of **Mn** can also be attributed to its ability to scavenge S and form high melting point sulfides. This reduces the available S in the alloy that can form low melting point Ni_3S_2, which gives rise to high temperature grain boundary embrittlement of Ni-Cr alloys [39].

Zirconium performs a similar role, scavenging O and S, and is known to provide improved high temperature tensile ductility and strength, creep life and rupture strength, and dwell crack growth resistance [40-4 2]. The S content in the small scale heats for producing powder was l 0 ppm for the development alloys and RRlO00.

There was no cause to significantly alter the level of C in the development alloys from that in RRlO00. However, B content was increased compared to that in RR lO00, which was defined for ingot as well as powder metallur gy. The aim of the higher B value was to produce beneficial grain boundary cohesion and toughness from elemental B or iso- lated M_3B_2 boride particles [40-4 2] but without reducing the precipitation of intergranular secondary γ' .

Iron was intentionally added to the development alloys at a level of about 1 at. % to facilitate the use of solid scrap from powder billet and machining chips in alloy manufac- ture. It was considered that such levels of iron would not be detrimental to alloy stability, and would behave like Co in reducing γ' T solvu s.

Material Manufacture

Powder of the development compositions and RR I 000 were produced at Allegheny Technologies Incorporated (ATI) Specialty Materials (Robinson) in Pittsburgh, PA, USA. These were sieved to a final screen size of -270 mesh (53 µm), filled into 3 inch diameter mild steel containers and hot isostatic pressed (HIP). End slices from the HIP com- pacts were used for experimental work to verify γ' Tsolvus values , and to evaluate phase stability and oxidation damage from stress-free thermal exposures at temperatures up to 800 °C. Bars of 76 mm in height and about 67 mm in diameter were machined from the compacts for isothermal forging at ATI Forged Products in Cudahy, WI, USA. The bars were forged down to a height of about 18 mm. From these, circular section test piece cylinders were extracted at mid-height locations for heat treatment. Solution heat treatment was conducted at 20 °C above the γ' Tsolvus followed by cooling at a nominal rate of 1.1 °C/s ± 0.3 °C/s between T,olvus and Tsolvus-90 °C. **RR**1000 cylinders were then given a post-solution heat treatment **(P-SHT)** of 16 h at 760 °C

and static air cooled. Cylinders of Alloy 1 and 2 received a P-SHT of 2 h at 850 °C, followed by 4 h at 800 °C, then static air cooled.

Experimental Work

Prior to forging and heat treatment work, differential scanning calorimetry (DSC) and heat treatment trials were undertaken to determine the γ' T s ol vus and the incipient melting temperatures. For DSC, a 5 mm diameter x 1 mm thick disk was cut from as-HIP material for each alloy and tested with a heating/cooling rate of 10 °C/min under flowing Ar.

Samples for isothermal oxidation and thermal exposure tests were also prepared from as-HIP material, which was subsequently heat treated to conditions stated in the material manufacture section. These samples were 20 x JO x 2 mm in size with chamfered edges on the faces of interest. At least one of these surfaces was polished to a 6 µm finish using diamond solution. The samples were held in open alumina boats and exposed in bench top furnaces at 800 °C for times up to 1000 h. Samples for assessment of phase stability were encapsulated in glass tubes under Ar and exposed in the same or similar furnaces. Following thermal exposure, oxide phases in Alloy 1 were identified using X-ray diffraction with a Cu Ka source. To protect the oxide scale during sectioning and metallographic preparation, samples were sputter coated with gold and electroplated with either Ni or Cu. Sections from oxidation and phase stability samples were prepared for scanning electron microscopy using SiC paper and diamond solution or colloidal silica (for Alloy 2). An electrolytic extraction was undertaken on the phase sta- bility sample for Alloy 2 according to ASTM E963-95 [43]. X-ray diffraction was conducted on the extracted residue using a Cu Ka source and a Ni filter .

After heat treatment, samples from forged material were prepared using standard metallographic techniques for characterization of microstructure. After polishing to a 0.10 µm finish using alumina solution, samples were electrolytically etched using 10% phosphoric acid solution. An optical microscope was used to acquire micrographs for grain size analy ses. From these, grain boundaries were traced manually to enable the determination of grain areas and subsequent calculation of equivalent diameter values. Gamma prime precipitates were characterized using ImageJ Software from at least 5 backscattered electron images that were taken during examination of polished samples . As reported previously [44], the size and area fraction of tertiary γ' precipitates that were determined from this method were found to be comparable to those from high resolution scanning transmission electron microscopy (STEM).

Round bar laboratory test pieces, with a gage diameter of 4 mm, were machined from the near net sized cylinders for tensile and creep testing. They had 2 ridges along the parallel section, 20 mm apart, which enabled an extensometer to be attached. Tensile testing was performed at room temperature, 600, 700 and 800 °C at a constant strain rate of 0.01 per s. Creep testing was conducted at 650 °C with a stress of 1000 MPa, at 700 °C with a stress of 800 MPa, at 750°C with a stress of 600 MPa and at 800 °C with a stress of 300 MPa. Due to the limited material , only a single test piece could be evaluated for each test condition.

Crack growth behavior was evaluated at 700 °C in square section 5 x 5 mm corner crack test pieces using a direct current potential difference technique, with electrodes wel- ded either side of a 0.1 mm wide starter slit. Test pieces were initially pre-cracked at room temperature before they were heated to 700 °C and subject to about 2000 baseline (0.25 Hz) fatigue cycles at a stress ratio of 0.1 and a peak load of 12 kN. Dwell cycles were then applied from a stress intensity factor range **(K)** of about 15 to 30 MPa./iu. These were trapezoidal waveforms (l-X-1-1) in which X was a hold period of 3600 s at peak load, also at 12 kN. Where possible, tests were completed after a further period of baseline fatigue cycles.

Results from the Experimental Work

The findings from DSC and heat treatment trials showed that the temperature for complete dissolution of γ' was found to be about 1160-1165 °C for both development alloys and about 1145-1150 °C for RRlOOO. Simi larly, the onset of incipient melting was detected at temperatures over 1200 °C for all of the alJoys, typically about 1210 °C. These latter values are very close to the predictions in Table 2.

Average grain size values of forged material after heat treatment are summarized in Table 3, with average size and volume fraction data for secondary and tertiary γ' precipi- tates. Values for one standard deviation are also provided in Table 3. The data confirm that a consistent grain size of about 20 µm was produced. The shape and size of γ' pre- cipitates in the 3 alloys can be understood from the backscattered electron images in Fig. l. They show that secondary γ' precipitates in the development alloys are more irregular in shape than those in RRlOOO, are larger in size and have a greater number density. RRlOOO has a higher volume fraction of tertiary γ' precipitates, which are about a half or one-third of the size of those in Alloy 1 and 2.

Data from tensile tests at room temperature and 800 °C are presented in Fig. 2 in the form of 0.2% proof stress (Rp0.2%) and tensile strength (Rm) values for the 2 devel- opment alloy compositions and RRlOOO. Whilst the tensile

Table 3 Results from characterization of mic rostructure . SGP and TGP are secondary and tertiary γ' respectively

	Measured dT/dt (°C/s)	Average size (diameter)			γ' volume fraction (%)		
		Gamma grain (μm)	SGP (nm)	TGP (nm)	SGP	TGP	Total
Alloy 1	0.9 ± 0.1	20.6 ± 0.5	273 ± 8	23.7 ± 0.7	52.4 ± 1.0	1.2 ± 0.1	53.6 ± 1.0
Alloy 2	1.4 ± 0.1	21.6 ± 0.2	238 ± 7	30.8 ± 1.4	50.7 ± 0.7	1.9 ± 0.4	52.5 ± 0.5
RRlO00	l.l ± 0.2	18.2 ± 0.6	149 ± 4	10.3 ±0.1	39.3 ± 0.6	4.5 ± l.l	43.8 ± 1.8

Values for one standard deviation follow average va lue s. Over 600 and 3000 SGP and TGP particles, respectively, were measured for each alloy

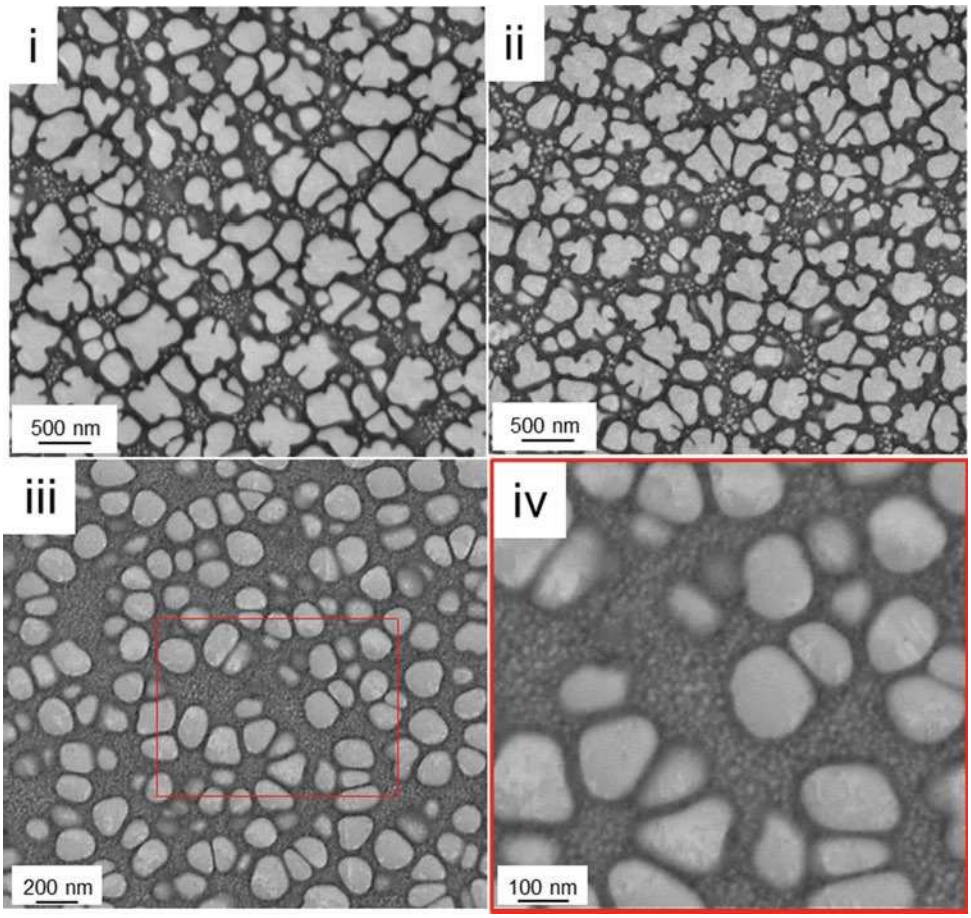

Fig. 1 Backscattered electron images of γ' precipitates after heat treatment for (i) Alloy l, (ii) Alloy 2 and (iii) RRlO00 at a magnification of x20,000. Image (iv) is a x 100, 000 magnification image of the red box in (iii)

strength properties of Alloy 1 are similar to those for RRlO00, the data show that Alloy 2 provides useful improvements over RRlO00.

Creep rupture life data for the development alloys and RRlO00 are compared using the Larson-Miller Parameter (LMP) in Fig. 3, where

$$\mathrm{LMP} = \frac{(273 + 8)(28 + \log t)}{1000} \qquad (5)$$

in which 8 is temperature and t is the creep rupture life. It is evident that Alloy 2 shows improved creep rupture life compared to RRlO00. Alloy 1, however, produced very similar creep rupture lives to those from RRlO00. Creep strain data for one of the test conditions (700 °C, 800 MPa) are plotted in Fig. 4. There is a significant difference in the shape of the creep curves for these alloys. Alloy 1 accumulates creep strain much faster than RRlO00 and Alloy 2, which show similar creep strain behavior up until about 0.4-0.5% creep strain. Further creep deformation appears to result in much faster rates of damage accumulation in RRlO00 than in Alloy2.

The results of crack growth testing are plotted in Fig. 5 in terms of crack growth rate per cycle (da/dN) versus stress intensity factor range (K). The data show that a significant

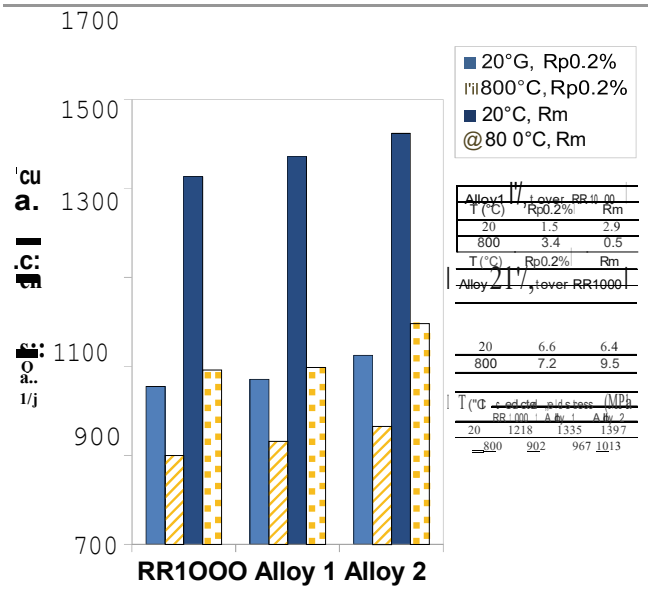

Fig. 2 0.2% proof stress (Rp0.2%) and tensile strength (Rm) data for Alloy 1, Alloy 2 and RRlO00 at 20 and 800 °C. Predicted values of yield stress from equation [3] are shown in the lower right table

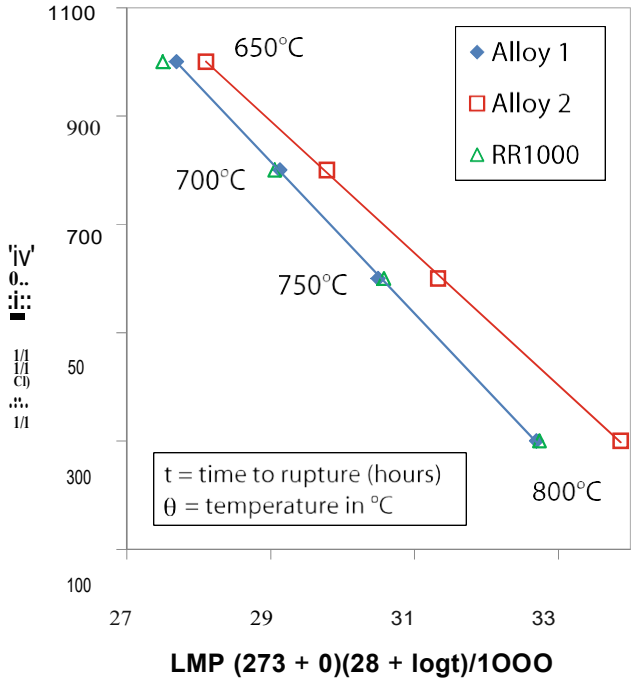

Fig. 3 Time to creep rupture data for Alloy 1, Alloy 2 and RRlO00 shown in terms of the Larson-Miller Parameter (LMP) from creep tests at 650, 700, 750 and 800 °C

increase in growth rate is produced in all of the alloys on the application of 3600 s dwell cycles at AK values of about 18 MPafrn. Subsequently, however, cracks were found to retard rapidly, *i.e.* reduced rates of crack growth were observed with increasing AK. To ensure that tests continued, baseline cycles were re-applied to AK values of about 23-25 MPafrn. At which point, dwell cycles were continued, with high rates of crack growth that were approximately 35

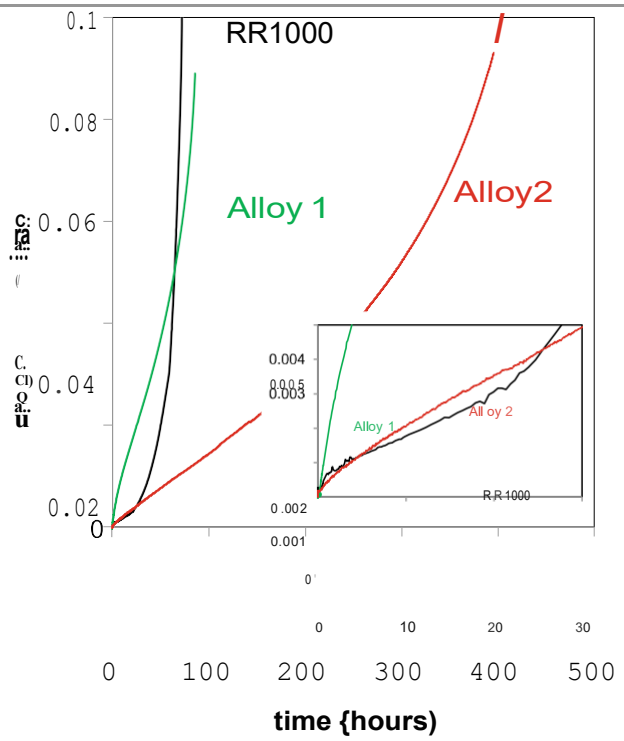

Fig. 4 Creep strain data measured from tests at 700 °C with a nominal stress of 800 MPa

times faster than those from baseline cycles. It is interesting to note that the crack in the Alloy 1 test piece showed another period of crack retardation to a AK of about 27 MPafrn and then started to grow in the expected manner, showing increases in growth rate with increasing AK. In contrast, cracks in the Alloy 2 and RRlO00 test pieces continued to accelerate, with the highest rates of crack

growth in the Alloy 2 test pieces . Examination of fracture surfaces in a SEM confirmed that intergranular crack growth occurred from all 3600 s dwell cycles, even during crack retardation.

Scanning electron microscope images of oxidation dam- age on polished surfaces of Alloy 1 and 2 after 1000 h at 800 °C are shown in Fig. 6. Previous work [36) on RRlO00 has identified that the outer scale consists of rutile (TiO_2) then chromia (Cr_2O_3) . Beneath these, there is internal oxi- dation damage in the form of alumina (Al_2O_3) intrusions. Both of the development alloys also displayed these oxida-

tion products but their depths were smaller than those for RRlO00, which are indicated in Fig. 6 by the red arrows that are labelled 1 and 2 for the scale and alumina intrusions respectively. The data for RRlO00 were taken from experi- mental work reported in [36, 45). The comparison shows that whilst both development alloys offer improved oxida- tion resistance, the improvement is most significant for Alloy 2. The resolution of the Alloy 1 image in Fig. 6 does not allow further insights into oxidation products or indi- cations of elemental migration. However, the results from X-ray diffraction in Fig. 6 show the presence of Cr_2MnO_4 spinel in the scale in addition to rutile and chromia.

Fig. 5 Crack growth rate *(da/dN)* versus stress intensity factor range (*!:iK)* data for Alloy 1, Alloy 2 and RRlO00 at 700 °C from testing in air using baseline **(1-1-1-1** s) and dwell (1-3600-1-1 s) cycles

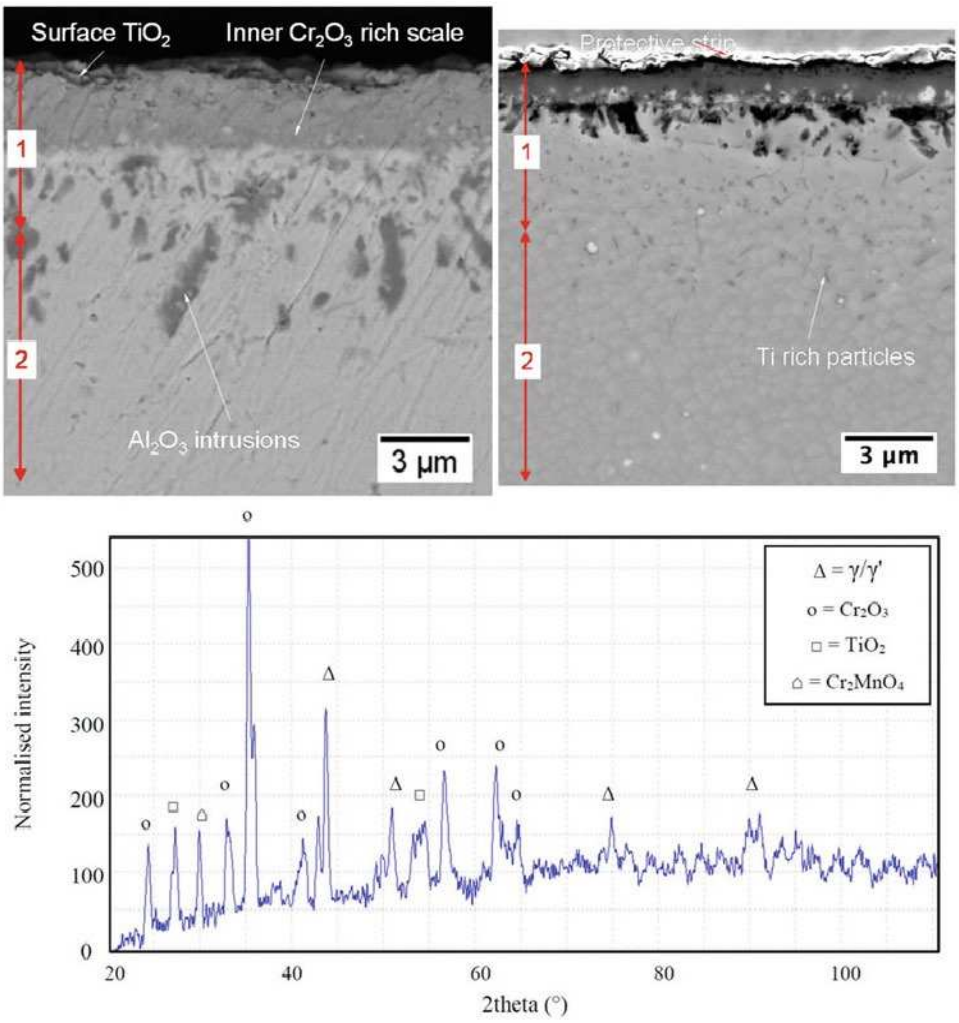

Fig. 6 Secondary electron image of oxidation products in Alloy **l** (top left) on a polished surface after 1000 h at 800 °C. Backscattered electron image of oxidation products in Alloy 2 (top right) on a polished surface after 1000 h at 800 °C. The red arrows are the depths of scale (1) and alumina intrusion (2) respectively that were measured after an identical exposure on a polished coarse RRlO00 surface [36, 45]. Lower chart shows X-ray diffraction data from a polished Alloy 1 sample after 1000 h at 800 °C

It has recently been reported that RRlO00 is free of undesirable TCP phases after a thermal exposure of 1000 h at 800 °C [46]. In con trast, the backscattered electron image in Fig. 9 shows that extensive grain boundary decoration was present in Alloy 1 after a 750 h exposure at 800 °C. Evidence in terms of a selected area electron diffraction pattern from TEM has confirmed that this phase, rich in Mo, Nb, Co, Cr, Fe, Wand Ta, was Cl4 Laves phase. There was little or no decoration of grain or prior particle boundaries in Alloy 2. Bright particles were present in backscattered electron images. From EDS, these were found to be either rich in Ti, Ta, Nb and C or rich in Mo and B but depleted in Ni, Co and Cr. X-ray diffraction confirmed that the former were MC carbides but peaks, presumably for Mo rich bor- ides, were not identified.

Discussion

Whilst a consistent grain size has been produced in the experimental material, measured cooling rates (Table 3) were unfortunately found to be at the ends and middle of the expected variation. This has been at the detriment of tensile and creep properties for Alloy 1 but to the benefit of Alloy 2. As such the average size of secondary γ' precipitates for Alloy l was larger than that for Alloy 2 and RRlO00. Given the low predicted misfit value (Table 2), wruch has been found to agree well with experimental measurements [47], it is possible that Alloy 1 is particularly susceptible to the anomalous coarsening and splitting phenomenon that was identified by Mitchell et al. [48, 49] during aging of RRlO00 at 800 °C. Such behavior may have grown the secondary γ' precipitates at the expense of tertiary γ' p articles, both in terms of size and volume fraction. The shape of secondary γ' precipitates in Fig. 1 (ii) also suggest that this phenomenon occurs in Alloy 2.

The differences in cooling rate and consequently sec- ondary γ' si ze, are likely to be major contributors to the observed differences in tensile and creep properties between Alloy 1 and Alloy 2. The trends are similar to those reported by other workers, notably Groh [50] for Waspaloy , in which improved properties were achieved by a higher cooling rate from solution heat treatment. Predicted values of yield stress are included in Fig. 2. These were calculated from equation [3], using the method described in [13, 27] for determination of APB energy and the data in Table 3. The model correctly predicts the trends in yield stress behavior that is observed in these alloys after heat treatment. Furthermore , if the grain size and the size distribution of secondary γ' particles were the same in Alloys 1 and 2, the model indicates that the yield stress value for Alloy 1 at 20 °C is within 32 MPa of the predicted value for Alloy 2 in Fig. 2.

Whilst the size and number density of tertiary γ' precip- itates are not included in equation [3] for predicting yield stress, these aspects of microstructure are critical for mini- mizing the accumulation of creep strain during sustained load tests or conversely, for beneficial stress relaxation behavior during sustained strain tests. This is evident from Fig. 4. RRlO00 has a lower volume fraction of γ' than the development alloys, by 8-10%, but offers a competitive resistance to creep strain accumulative at the selected test conditions (700 °C, 800 MPa) as a result of a relatively high volume fraction of fine tertiary γ' precipitates. Alloy 2 shows very similar creep strain versus time data to RRlO00 although the spaces between the secondary γ' precipitates are smaller in Alloy 2 but the size of tertiary γ' precipitates is a factor of 3 larger and there are fewer of them. Howeve r, Alloy 2 shows improved resistance to creep above strains of 0.4- 0.5%. It appears that significant creep damage occurs at lower creep strains in RR LO00 than in Alloy 2. It is postu- lated that such damage nucleates from grain boundary par- ticles such as carbides, borides or oxides. RRl000 has fewer borides that may pin grain boundaries and hinder grain boundary displacement but it shows a significantly higher concentration of small oxide particles, due to the Hf content in the alloy. Alloy 1 accumulates creep strain much faster than the other 2 alloys. This is likely to result from having larger secondary γ' precipitates and the smallest volume fraction of tertiary γ' precipitates. The observed effects of γ' size and volume fraction can be predicted using the Orowan model adapted by Galindo-Nava and Rae [51]. Evidence is not presented here but has been reported by Christofidou et al. [27] for other development compositions. The inferior creep performance of Alloy 1 is not considered to result from phase instability as Laves phase was not detected after long term exposures at 700 °C.

The inelastic deformation behavior shown by Alloy 1 is beneficial during dwell crack growth testing. This is because nominally elastic material constrains the inelastic zone around the crack tip and imposes an essentially strain con-trolled loading configuration at the crack tip. Under these conditions, the crack tip stresses in Alloy 1 are able to decay much faster during the sustained load than those in Alloy 2. The behavior of the development alloys shown in Fig. 5 is consistent with the findings of previous work that have investigated the effects of microstructure on dwell crack growth rates [44, 52- 54]. In coarse grain microstructures, in particular, it has been found that cracks at low values of K retard during dwell cycles. It is understood that oxide intrusions form ahead of a stationary or a slow growing crack, with an increase in volume that induces compressive stresses in the matrix in the vicinity of the crack tip [55]. This and crack blunting from inelastic deformation are likely causes of the observed retardation behavior. Significantly

higher growth rates are produced at K values greater than 25 MPa./m from continuous intergranular crack growth. Further evidence is required to understand the mechanisms that give rise to this behavior. It is encouraging, however, to find that development alloys, which contain a higher number density of γ' precipitates and have higher yield stress values than RRlO00 show similar time dependent crack growth behavior at 700 °C.

The images in Figs. 6 and 7 indicate that the development alJoys have improved resistance to oxidation damage compared to RRlO00. Although the reduced Ti content and the slightly higher Cr/Ti ratio in the new alloys may contribute signific antly to this improvement, more detailed investigations are necessary to identify the presence of Ta oxides [56] and SiO_2 particles below the chromia scale. Similarly, the importance of Cr_2MnO_4 spine l in the scale of Alloy 1 needs to be understood but is beyond the scope of the current study.

Alloy l was shown to precipitate Cl4 Laves phase after long term exposure at 800 °C while Alloy 2 and RRlO00 were found to not to form undesired TCP phases. Interest- ingly, none of the alloys precipitated CJ phase, which for these alloys supports the use of phase diagram modelling to predict CJ Tsolvu s and y composition for average Mdy values. It has been established [57] that additions of 0.5 and l wt% Si. to cast B-1900, 713C and MAR-M200 produce hexag- onal Mo(Ni,Sih Laves phase during solidification. However, the reduced amount of Si in Alloy 2 did not lead to the precipitation of Laves phase. It should also be noted that a similar development alloy, D8 in reference [58] also precipitated Laves phase but it contained no Si. It did contain 0.9 wt% Fe and high levels of Nb, W and Cr, with moderate additions of Mo.

Summary

This paper examined 2 new alloy compositions ,which were designed for possible disk rotor applications. Both were intended to have higher γ' content than the existing alloy, RRlO00, and be produced using powder metallurgy and isothermal forging to enable forgings to be made that show a consistent coarse grain microstructure. Small pancake forgings of the new alloys and RRlO00 were made and from

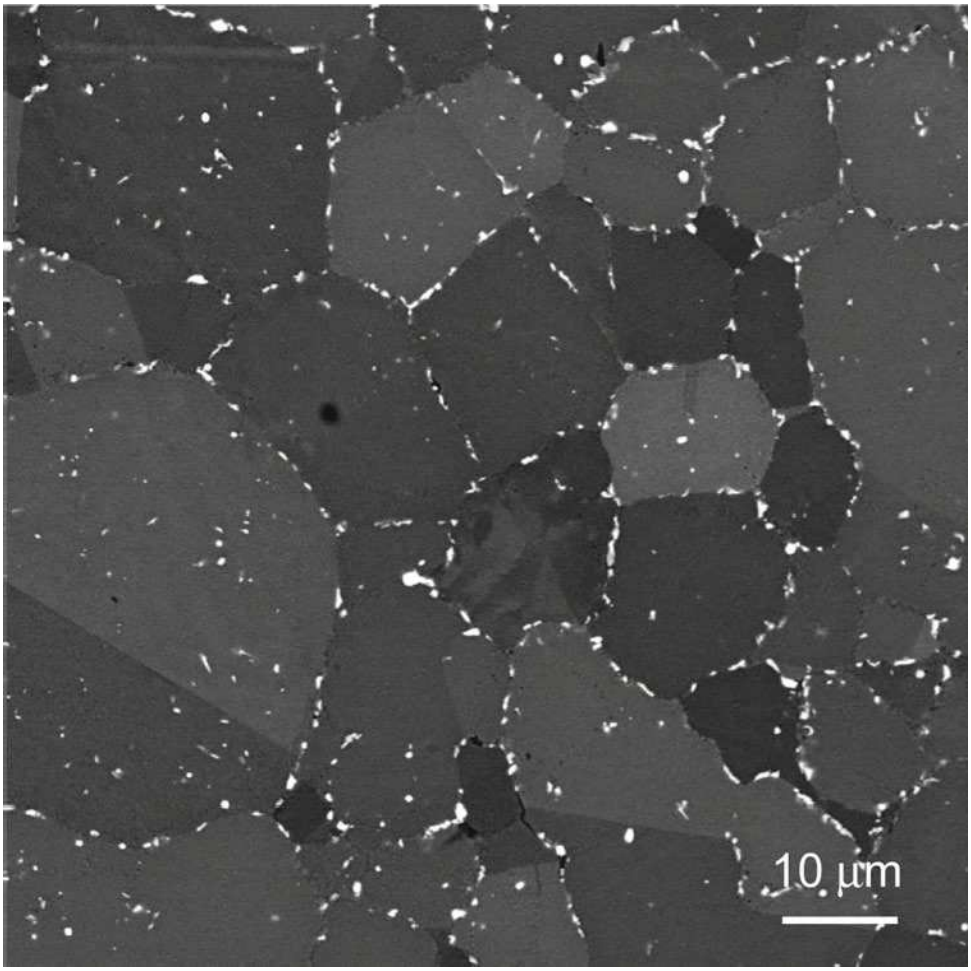

Fig. 7 Backscattered electron image of Alloy 1 after 750 h at 800 °C

these, blanks were solution heat treated, cooled at measured rates and aged. The development alloys were similar in composition but they exhibited different tensile and creep properties, phase stability and resistance to oxidation damage. Despite attempts to minimize variation in rnicrostructure from heat treatment, differences in γ' size distribution were found to influence tensile and creep behavior. One of the new alloys (Alloy 2) showed improved yield and tensile strength compared to coarse grain RR1000. Alloy 2 displayed similar initial creep strain behavior to RRlO00 but superior resistance to subsequent creep damage, producing longer creep rupture lives. All of the alloys showed crack retardation at low stress intensity factor ranges *(11K)* from 3600 s dwell cycles at 700 °C in air. This occurred whilst crack growth was intergranular. In agreement with work in the literature, this behavior was attributed to relaxation of crack tip stresses and the development of compressive crack tip stresses from the formation of crack tip oxide intrusions . At higher *11K* values, the rates of continuous dwell crack growth in the development alloys were similar to those in coarse grain RRlO00 although the new alloys showed a higher number density of γ' precipitates. Alloy 1 was found to precipitate C14 Laves phase from long term exposure at 800 °C. This was considered to be due to excessive Si content in an alloy that contained high levels of Mo, W, Cr and Nb. Like RRlO00, cr phase was not detected in the new alloys after 750 h at 800 °C.

Acknowledgements This work was supported by Rolls-Royce pie and the Rolls-Royce/EPSRC Strategic Partnership under EP/H022309/1, EP/H500375/l and EP/M00560 7/l. Dr Hardy wou ld li ke to thank Ro lls-Royce colleague Dr Han Tai for his support and enco uragement in this work, Professor Roger Reed and Dr David Crudden from the University of Oxford for fruitful discussions and Mr Joe Muha, formerly of ATI Specialty Materials, Rob inson , for his assis tance in making the powder compacts.

References

1. European Commission, (2001), European Aeronautics: A Vision for 2020.
2. European Commission, (2011), Flightpath 2050 Europe's vision for aviation. https://doi.org /10.2777/50266.
3. Reed RC , Mottura A, Crudden DJ, (2016), Alloys-by -de sig n: towards optimization of compositions of nickel-based supera lloys. In: Superalloys 2016, (Ed. by Hardy MC *et al.),* TMS, Warrendale , p 15-23.
4. Mitchell RJ, Lemsky JA , Ramanathan R, Li HY, Perkins KM and Connor LD, (2008), Process development & microstructu re & mechanical property eva l uation of a dual microstructure heat treated advanced nickel disc alloy. In: Superalloys 2008, (Ed. by Reed RC *et al.),* TMS, Warrendale, p 347-356.
5. https://www.ic ao.int/Meetings /Env iro nmen talWorkshop s/Documents/ ICAO-TransportCanada-2006/Anderson_ops.pdf.
6. Dreshfield RL, Gray HR, (1984), *PIM Superalloys - a Troubled Adolescent,* NASA Technical Memorandum, TM-83623 , Lewis Research Center, Cleveland.
7. Anderson R, (1990), Powder Metallurgy at Pratt and Whitney , The International Jou rnal of Powder Metallurgy , 26, (2):171-178.
8. Smythe S, (2008), Superalloy powders: an amazing history , Advanced Materials and Processes, November: 52-55. https:// www.asminternational.org/documents/ IOl 92/1887146/ampl 6611 p052.pdf/6664af73-fa87-4c2f-8b94-d420d5c438e3/ AMPl66 l lP052.
9. Hardy MC, Zirbel B, Shen G, Shankar R, (2004), Developing damage tolerance and creep resistance in a high strength nickel alloy for disc appli catio ns. In: Superalloys 2004, (Ed. by Green KA et al.), TMS, Warrendale , p 83 -90.
10. Reppich B, (1982), Some new aspects concerning particle hardening mechanisms in γ' precipitating Ni-based alloys - I. theoretical concept, Acta Metall., 30:87-94.
11. Parthasarathy TA, Rao SI, Dirniduk DM, (2004), A fast spread- sheet model for the yield strength of supe ralloys. In: Superalloys 2004, (Ed. by Green KA *et al.),* TMS, Warrendale, p 887-896.
12. Kozar RW , Suzuki S, Milligan WW, Schira JJ, Savage MF, Pollock TM, (2009), Strengthening mechanisms in polycrystalline multimodal nic kel- base superalloys , Met. Trans. A, 40, (7):1588-1603.
13. Crudden DJ, Mottura A, Warnken N, Raeisinia B, Reed RC , (2014), Modelling of the influence of alloy composition on flow stress of high-strength nickel-based supera llo ys, Acta Mater., 75:356- 370.
14. Galindo-Nava El, Connor LD, Rae CMF, (2015), On the prediction of the yield stress of unimodal and multimodal γ' nickel-base superalloys, Acta Mater., 98:377-390.
15. Hardy M, Reed R, Crudden D, (2018), European Patent Specification EP 3 112 485 Bl , 15 August 2018.
16. Hardy MC, Reed RC, Crudden D, (2019), United States Patent US I 0,266,919 B2, 23 April 20 I 9.
17. Hardy MC, Reed RC, Crudden D, (2019), United States Patent US 10,422,024 B2, 24 September 2019.
18. Saunders N, (1996), Phase diagram calculating for Ni-Based Superalloys. In: SuperalJoys 1996, (Ed. by Kissinger RD *et al.),* TMS, Warre nd ale, PA, USA, p 101-110.
19. Small CJ, Saunders N, (1999), The application of CALPHAD techniques in the development of a new gas-turb ine dis k alloy, MRS Bulletin , 24, (4): 22-26.
20. Saunders N, Fahrmann M, Small CJ, (2000), The appli catio n of CALPHAD calculations to Ni-Based Superalloys. In: Superalloys 2000, (Ed. by Pollock TM *et al.),* Warrendale, p 803-81 l.
21. Antonov S, Detrois M, Helmink RC , Tin S, (2015), Precipitate phase stability and compositional dependence on alloying addi- tions in y-γ' -0-TJ Ni-based supe ralloys , Journal of Alloys and Compounds , 626:76- 86.
22. Telesman J, Kant zos P, Gayda J, Bonacuse PJ, Prescenzi A, (2004), Microstructural variables controlling time-dependent crack growth in a P/M supe ralloy. In: *Superalloys 2004,* (Ed. by Green KA *et al.),* TMS, Warrendale, p 215-224.
23. Evans HE, (1988), Cavity formation and metallurgical changes induced by growth of oxide scale , Materials Science and Technology , 4, (12):1089-1098.
24. Sudbrack CK, Evans LJ, Garg A, Perea DE and Schreiber DK, (2016), Characterization of grain boundar ie s and associated minor phases in disk alloy ME3 exposed at 815 °C. In: Supe ralloys 2016, (Ed. by Hardy MC *et al.),* T MS, Warrendale, p 927-936.
25. Con no lley T, Starink MJ, Reed PAS, (2000), Effect of oxidation on high temperature fatigue crack initiation and short crack growth in lnconel 718. In: Superalloys 2000, (Ed. by Pollock TM et al.), TMS, Warre ndale , p 435-444.

26. Huron ES, Bain KR, Mourer DP, Gabb T, (2008), Development of high temperature capability P/M disk superalloys. In: Superalloys 2008, (Ed. by Reed RC *et al.),* TMS, Warrendale , p 181-189.
27. Christofidou KA, Hardy MC, Li HY, Argyrakis C, Kitaguchi H, Jones NG, Mignanelli PM, Wilson AS, Messe OMDM, Picker- ing EJ, Gilbert RJ, Rae CMF, Yu S, Evans A, Child D, Bowen P and Stone HJ, Met. Trans., 49A (9):3896- 3907 .
28. Tien JK , Jarrett RN, (1983), *Effects of Cobalt in Nickel-Base Superalloys,* NASA Contractor Report CR168308 , NASA Lewis Research Center, Cleveland.
29. Luthra KL, (1982), Low temperature hot corrosion of cobalt-base alloys: part I. morphology of the reaction product, Met. Trans. A, 13, (10):1843-1852.
30. Lillerud KP, Kofstad P, (1984), Sulfate-Induced hot corrosion of nickel, Oxidation of Metals, 21, (5/6):233-270.
31. Reed RC, (2009), *The Superalloys, Fundamentals and Applications,* Chapter 2, Cambridge University Press, ISBN 9780511541285, https://doi.o rg/10.1017 /CBO9780511541285.
32. Randle V, (1997), Mechanism of twinning-induced grain boundary engineering in low stacking-fault energy materi als, Acta Mater., 47, (15):4187-4196.
33. Christofidou KA, Jones NG, Pickering EJ, Flacau R, Hardy MC, Stone HJ, (2016), The microstructure and hardness of Ni-Co-Al-Ti-Cr quinary alloys, Journal of Alloys and Compounds , 688:542-552.
34. Morinaga M, Yukawa N, Adachi H, Ezakil H, (1984), New PHACOMP and its application to alloy design. ln: Super- alloys 1984, (Ed. by Gell *Met al.),* TMS, Warrendale , p 523-532.
35. Guedou J-Y, Augustins-Lecallier I, Naze L, Caron P, Locq D, (2008), Development of a new Fatigue and creep resistant PM nickel-base superalloy for disk applications. In: Superalloys 2008, (Ed. by Reed RC *et al.),* TMS, Warrenda le , p 21- 30.
36. Cruchley C, Evans HE, Taylor MP, Hardy MC, Stekovic S, (2013), Chromia layer growth on a Ni-based superalloy: sub-pa rabolic kinetics and the role of titanium , Corrosion Science, 75:58-66.
37. Pedrazzini S, Rowlands BS, Turk A, Parr IMD, Hardy MC, Bagot PAJ, Moody MP, Galindo-Nava E, Stone HJ, (2019), Partitioning of Ti and kinetic growth predictions on the thermally grown chromia scale of a polycrystalline nickel-ba sed superalloy , Met. Trans A., 50, (7):3024-3029.
38. Pedrazzini SD, Child DJ, West G, Doak SS, Hardy MC, Moody MP, Bagot PAJ, (2016), Oxidation behaviour of a next generation polycrystalline Mn containing Ni-based supe ralloy, Scripta Materiali a, 113:51-54.
39. White CL, Schneibel JH , Padgett RA , (1983), High temperature embrittlement of Ni and Ni-Cr alloys by trace elements, Met. Trans. A, 14, (4):595-610.
40. Gayda J, Gabb TP, Miner RV, (1985), *Fatigue Crack Propagation of Nickel-Base Superalloys at 650* °C, NASA Technical Memorandum 87150, NASA Lewis Research Center, Cleveland.
41. Garosshen TJ, Tillman TD, McCarthy GP, (1987), Effects ofB, C, Zr on the structure and properties of a PIM nickel base superalloy , Met. Trans. A, 18, (1):69-77.
42. Jain SK, Ewing BA, Yin CA, (2000), The development of improved performance PM Udimet® 720 turbine dis ks. In: Superalloys 2000, (Ed. by Pollock TM *et al.),* TMS, Warrendale, p 785-794.
43. ASTM E963-95, *Standard Pra ctice for Electrolytic Extraction of Phases from Ni and Ni-Fe Base Superalloys Using a Hydrochloric-Methanol Electrolyte,* ASTM International, West Conshohocken.
44. Shulz F, Li HY, Kitaguchi H, Child D, Williams S, Bowen P, (2018), Influence of tertiary gamma prime (γ′) size evolution on the dwell crack growth behaviour in CG RRIO00, Met. Trans. A, 49, (9):3874-3884.
45. Cruchley S, Taylor MP, Evans HE, Hardy MC, Child DJ, (2014), Characterisation of subsurface oxidation damage in Ni based super alloy, RRIO00, Materials Science and Technology, 30, (15):1884-1889.
46. Wilson AS, Christofidou KA, Evans A, Hardy MC, Stone HJ, (2019), Comparison of methods for quantification of topologic ally closed packed phases in Ni-based superalloys, Met. Trans. A, 50, (12):5925-5934.
47. Papadaki C, (2019), *Optimising Creep Resistance of Next Gener- ation Nickel-Based Superalloys via Tailoring of γ′ Precipitates Using Different Heat Treatmems,* Confirmation of Status Report , Trinity College, University of Oxford, Oxford.
48. Mitchell RJ, Preuss **M,** (2007), Inter-relationships between the composition , γ′ mo rpholog y, hardnes s, and y-γ′ mis match in advanced polycrystalline nickel-base superalloys during aging at 800 °C, Met. Trans. A, 38, (3):615-627.
49. Chen **Y,** Prasath Babu R, Slater TJA, Bai M, Mitchell R, Ciuca 0 , Preuss M, Haigh **SJ,** (2016), Acta Materialia, 110:295-305.
50. Groh JR , (1996), Effect of cooling rate from solution heat treatment on Waspaloy microstructure and properties. In: Super- alloys 1996, (Ed. by Kissinger RD *et al.),* TMS, Warrendale, p 621-626.
51. Galindo-Nava EI, Rae CMF, (2016), Microstructure-senstive modelling of dislocation creep in polycrystalline FCC alloys: Orowan theory revisited, MSEA, 651:116-126.
52. Gabb TP, Gayda J, Telesman J, Garg A, (2008), The effects of heat treatment and mic rostructure variations on disk superalloy properties at high temperature. In: Superalloys 2008, (Ed. by Reed RC *et al.),* TMS, Warrendale, p 121-130.
53. Li HY, Sun JF, Hardy MC, Evans HE, Williams SJ, Dael TJA, Bowen P, (2015), Effects of microstructure on high temperature dwell fatigue crack growth in a coarse grain PM nickel based superalloy, Acta Mater., 90:355-369.
54. Telesman J, Gabb TP, Ghosn LS, (2016), Separating the influence of environment from stress relaxation effects on dwell fatigue crack growth in a nickel-base disk alloy. In: Superalloys 2016, (Ed. by Hardy MC *et al.),* TMS, Warrendale , p 55 1- 560 .
55. Evans HE, Li HY, Bowen P, (2013), A mechanism for stress-aided grain boundary oxidation ahead of cracks, Scripta Materialia, 69:79-182.
56. Sudbrack CK, Draper SL, Gorman TT, Telesman J, Gabb TP, Hull DR, (2012), Oxidation and the effects of high temperature exposures on notched fatigue life of an advanced powder metallurgy disk superalloy. In: Superalloys 2012, (Ed. by Huron ES *et al.),* TMS, Warrendale , PA, p863-872.
57. Miner RV Jr. (1977), Effects of silicon on the oxidation, hot-corrosion and mechanical behavior on two cast nickel-base superalloys, Met. Trans. A, 8, (12):1949-1954.
58. Reed R, Crudden D, Raeisinia B, Hardy M, (2016), European Patent Specification EP2 894 234 Bl , 19 October 2016.